Features of Internal Flow and Spray for a Multi-Hole Transparent Diesel Fuel Injector Tip

Russell P. Fitzgerald*[1], Giovanni Della Vecchia[2], Jesús E. Peraza[3], Glen C. Martin[1]
[1]Combustion & Thermofluids, Caterpillar, Inc., Mossville, IL, USA
[2]Combustion & Thermofluids, Caterpillar, Inc., Peterborough, UK
[3]Motores Térmicos. Universitat Politècnica de València, Valencia, Spain
*Corresponding author: Fitzgerald_Russell_P@cat.com

Abstract
The rise of fuel injector pressures in diesel engines has generally increased internal flow problems in the injector tip, particularly, the formation of cavitation vapor bubbles. These can not only impact spray formation, but their subsequent collapse can lead to cavitation erosion damage, affecting engine component life and performance. In this work, internal flow and spray phenomena are investigated for a multi-hole diesel fuel injector tip via flow visualization experiments and computational simulations of the flow injection event.

A multi-hole transparent quartz injector tip mated with a production injector body enables internal flow to be investigated for rail pressures up to 1000 bar. Effects of internal flow geometry, ambient (back) pressure, and rail pressure on the locations of vapor clouds and bubble inception are quantified via analysis of relatively high-speed (110kHz) imaging throughout needle opening, quasi-steady injection, and needle closing events.

Measured quantities from experiments, including local cavitation vapor probability and volume fraction are compared with computational simulations to enhance understanding of complex observed internal flow phenomena and to validate model predictions. Simulations employing volume-of-fluid (VOF) interface tracking and a homogeneous relaxation model (HRM) with fixed mesh refinement are also used to examine the effects of real geometry (as determined by high-resolution x-ray tomography) on internal flow predictions. Overall, this work represents a considerable effort to develop tools that will aid the design of robust hardware and spray combustion processes for injection pressures exceeding 2500 bar.

Keywords
Internal flow, cavitation, orifice, spray, diesel injector, imaging diagnostics

Introduction
Diesel fuel injectors are affected by cavitation and other internal flow phenomena, especially as operating pressures have risen well beyond 1000 bar to enhance mixing and to suppress pollutant formation. Erosion damage from vapor collapse is often the primary concern, as injector delivery is affected and fuel system robustness is compromised. Effects of cavitation and internal flow on spray formation is an important secondary concern.

These problems have motivated many efforts to detect, understand, and predict cavitation phenomena in diesel fuel injectors. Early work by others [1-4] focused on orifice inlet geometry effects on spray morphology, droplet size, velocity profiles, and flow. Analysis by Benajes [5] and Desantes [6] explored the relationship between non-dimensional flow coefficients and cavitation number as originally advocated by Nurick [7]. Understanding of internal flow and cavitation structure in scaled diesel injector tips has been enhanced by the experimental investigations of Kim [8], Soteriou [9-10], and Arcoumanis [11-12] for cylindrical and conical orifices. Predictive models of internal flow phenomena by Schmidt [13] and Ning [14] have also increased knowledge about vapor inception locations, asymmetric effects, and impact of cavitation on liquid length.

Despite the plethora of works delineating these phenomena, reliable screening approaches for real (i.e. multi-hole, production) geometries are still needed to answer: 1) How likely is vapor formation and erosion damage for a given geometry? 2) What geometric features are responsible? 3) What phase of the injection event is most critical? 4) To what degree does internal vapor affect spray? In this work, these questions are addressed by experimental and computational investigations of a transparent production injector tip at engine-relevant operating conditions.

Experimental Approach
To study internal flow and cavitation within a heavy-duty diesel fuel injector, a transparent tip has been designed and fabricated. Beginning with a 6x5x2mm^3 piece of quartz glass, production injector tip features have been ground and laser-drilled to include five k-factored orifices fed by an eccentric hemispherical sac (see Figures 1

and 2a). Conical orifices were drilled through relatively large counterbores in the sides of the transparent tip, allowing clearance for the exiting spray and simultaneous observation; although, in this work, spray from the transparent tip is not studied in detail. The counterbore is large enough that it has little effect on backpressure and upstream internal flow. Mating of the transparent tip with a metal production injector tip body has been achieved using optical adhesive combined with a spring-loaded assembly as shown in Figure 2b.

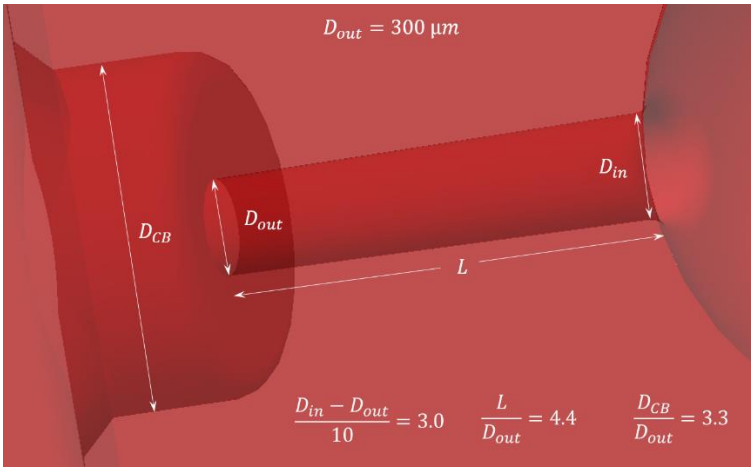

Figure 1. Transparent tip orifice geometry. Flow is from right to left.

Several internal geometric features are tested in this work to determine their propensity to cavitate or form vapor clouds within the sac and orifice regions. The baseline injector tip geometry (i.e. Injector 1) has a hydro-erosively ground orifice (i.e. HEO) to achieve a 20% flow increase via enlargement and rounding of the orifice inlet radius as it transitions from the sac. Injector 2 maintains the same sac and hole geometry, but includes an undisclosed, alternate seat/needle design. Known to suffer from cavitation erosion damage after many hours of operation, the performance of Injector 2 is compared to that of Injector 1 in this work to determine if such problems can be anticipated, studied, and predicted. Effects of the hydro-erosive processes (HEO) are also investigated in this work to quantify the probability and spatial distribution of vapor formed for sharp versus smooth inlet radii.

The transparent tip assembly is mounted in an unheated, windowed vessel, capable of experiments up to 30 bar ambient pressures as shown in Figure 2c. Additional details of the test vessel and imaging diagnostics are described in previous work [15]. Injector internal flow and spray are monitored through the transparent tip via high-speed (110kHz) imaging of visible light diffracted and scattered from the fluid. When no vapor is present in the liquid, light emanating from side- and back-adjacent sources passes through the transparent tip without disruption; consequently, the sac and holes are apparently clear as the quartz glass and liquid diesel fuel are index of refraction matched. When vapor is present, light rays are bent and detected as local, temporal high and low intensity (i.e. light and dark regions) in the image sequence. An image processing algorithm identifies vapor parcels via this approach by fitting each pixel-ensemble to a smooth time-varying intensity curve and then counting instances for which the local intensity deviates from the mean by more than an experimentally determined noise threshold. Using this approach, the time-varying probability of vapor can be quantified for each sac and orifice location from the vantage point of the camera.

As fluid pressures increase in a diesel fuel injector and flow restriction velocities rise precipitously, problems with cavitation and vapor formation tend to appear. The dimensionless cavitation number, K, defined as:

$$K = \frac{(P_i - P_v)}{P_i - P_a}, \tag{1}$$

quantifies the propensity to cavitate as injection pressure, P_i and ambient back pressure, P_a vary relative to the vapor pressure (P_v) of the working fluid as described for injector orifices in work by Nurick [7]. Plots of the cavitation number in Figure 3 illustrate the typical operating range for heavy duty diesel injectors within the cavitating regime for ambient pressures between 60 and 200 bar. The operating point with the highest cavitation propensity (i.e. a cavitation number closest to unity) is denoted in the plot by an open black circle at 2500 bar sac pressure and K near 1.03. Achieving the same minimum cavitation number in this work for an ambient pressure of 15 bar only requires sac (injection) pressures near 600 bar as indicated by the red circle denoted in Figure 3. Nevertheless, injection pressure is varied from 300 to 1000 bar (i.e. the upper practical limit of quartz material integrity) to investigate effects over a broader range of cavitation numbers. Addition of a test point at 30 bar

ambient pressure and 300 bar sac pressure enables the entire diesel injector operating range to be spanned as indicated by the red and blue filled asterisks shown in Figure 3.

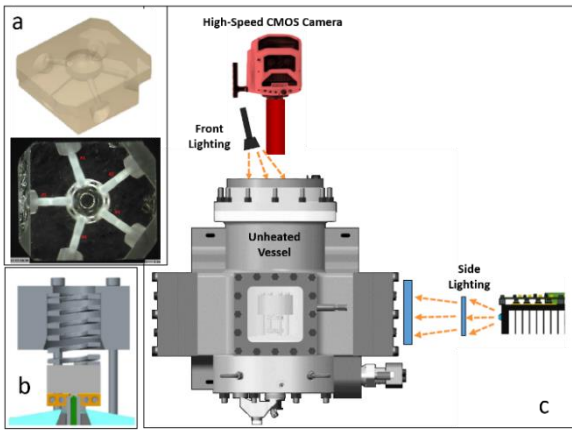

Figure 2. Illustration of a) transparent tip, b) injector rig assembly, c) test vessel for experiments

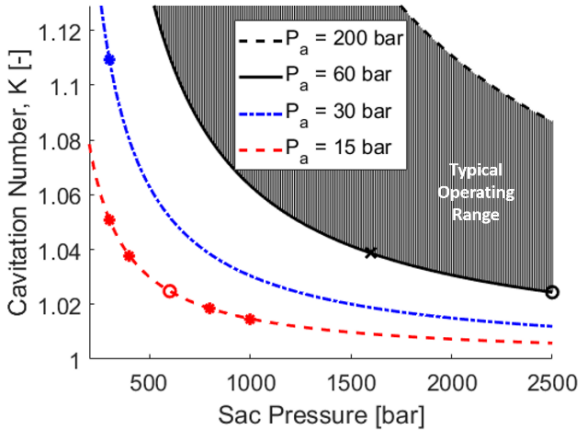

Figure 3. Cavitation domain map illustrating test conditions compared with injector conditions during engine operation.

Computational Approach

Three dimensional CFD simulations of the in-nozzle flow were performed using Converge 2.4 as described in [16-17]. All the simulations carried out in this work relied on a Reynolds-averaged Navier-Stokes formulation with the standard k-ε turbulence model. To model the multiphase changes due to cavitation, a Homogeneous Relaxation Model (HRM) through a volume-of-fluid (VOF) representation in the Eulerian framework was utilized as described in [18]. Compressible fluid and ideal gas properties from the Converge database were used to model fuel (diesel) liquid, vapor, and ambient gas phases.

All simulations performed in this study use the same CFD and grid setup. Experimentally measured vertical needle lift profiles were employed; whereas, needle wobble was neglected. The computational domain consists of the volume between injector and needle walls, the sac volume and the nozzle holes. A 20mm diameter hemispherical outlet domain was added at the exit of the nozzle hole to allow the flow to fully develop when exiting the orifices. Fixed embedding is required to refine the grid and capture the flow characteristics more accurately. Adaptive Mesh Refinement was not used. A spherical area of fixed embedding with grid size of 22.5 µm (minimum) was used in the passage between injector and needle walls, inside the orifices and in the near-nozzle regions. Grid size transitioned to 90 µm and 360 µm in the outer part of the outlet domain. This strategy maintains cell counts between 1.8 and 2.8 million as the needle moves relative to the seat. A logarithmic law-of-the-wall model was employed since the minimum grid size is insufficient to resolve the boundary layer.

Results

The gallery of images shown in Figure 4 represents a broad range of internal flow phenomena observed through the transparent tip during an injection event. Just prior to injection, the circular sac region sometimes includes previously entrained vapor bubbles from the ambient as pictured in the centre of Figure 4a similar to observations by Swantek [19] and Manin [20]. As the injector needle begins to lift, such bubbles often collapse or get pushed into the orifices. The large pressure difference across the needle seat generates high velocity flows. Many vapor bubbles are formed throughout the sac as evidenced by images like that in Figure 4b and the typically sharp initial rise in measured vapor probability apparent from all curves shown in Figure 5. After some time, the sac is generally cleared of bubbles as indicated by dashed lines in Figure 5, and a quasi-steady flow-field is established as pictured in Figures 3c-f. During this period, the overall vapor probability is usually lower. Vapor inception near the orifice inlets appears periodically (Figures 3c-d), as does string cavitation as shown in Figures 3e-f. The former features are also responsible for instantaneous fluctuations about a mean quasi-steady vapor probability during the steady portion of the curves in Figure 5. String vortices of cavitation are significantly shorter lived, appearing for 20-30µs in a manner similar to that described in [11]. These strings sometimes extend from one orifice to another (as in Figure 4e), or to the needle surface [21]. As the needle begins to close (as indicated by the solid lines at the bottom of Figure 5) and the flow is throttled, vapor bubbles rapidly form again in the sac (as indicated by the sharp rise in overall vapor probability near the end of the time-varying profiles shown in Figure 5). During the needle closing period, clouds of vapor originating from the orifice inlets fill the sac (as shown in Figure 4g), indicating likely ingestion of ambient gases. After some time, vapor bubbles in the sac coalesce and return to a stagnant condition prior to injection.

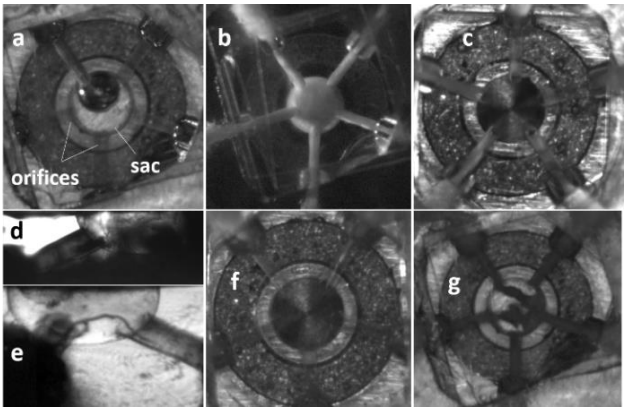

Figure 4. Gallery of images through transparent tip throughout injection

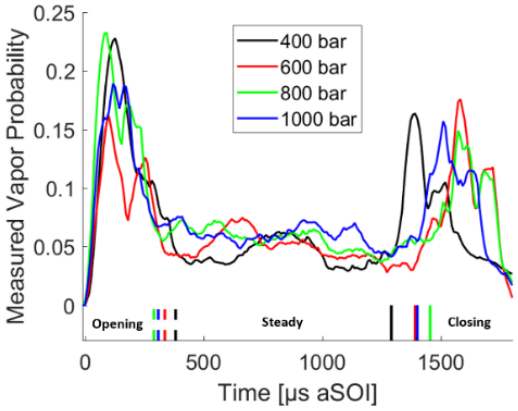

Figure 5. Estimates of time-varying vapor probability in sac/orifices for four different rail pressures. Dashed lines and solid lines indicate times of sac clearing and check closing, respectively.

Geometry Effects

Differences in transient vapor probability and its spatial distribution have been investigated for several injector tip geometries so as understand their effects on internal flow and cavitation. Effects of different needle/seat geometry are shown in Figures 6 and 8. Effects of hydro-erosive grind, i.e. HEO are summarized in Figures 7 and 9. Although Injectors 1 and 2 share a similar initial rise in the overall vapor probability during opening, periodically high levels persist throughout the entire event for Injector 2, which takes 200μs longer for the sac to clear. Consequently, it has a very brief quasi-steady period before ramping up to high vapor probability during closing. Maps of the spatial vapor probability are compared in Figure 8 for each of the three periods of injection; computed values of the spatially averaged vapor probability for each sac and orifice set are also listed as insets.

During the opening period, the two injectors exhibit similar distributions of vapor in the sac and orifices. Both distributions are asymmetric, with high levels of vapor inception within the orifice in the 6 o'clock position. This appears to be consistent with previous observations of internal flow-field disruption and asymmetry from needle wobble during opening [11, 22]. Differences are more pronounced during the two subsequent stages of injection, during which Injector 2 exhibits consistently higher vapor probability in both the sac and orifices. Injector 1 has very low vapor probability (i.e. 3-4%) during steady injection; whereas vapor levels are three times higher for Injector 2. Close examination of its steady cavitation probability map reveals strong vapor inception near the orifice inlets and rapidly diminishing levels about one diameter downstream, likely indicative of vapor cloud collapse and potential erosion. The differing needle geometry of Injector 2 further manifests itself during closing with more than double the vapor probability in most regions compared to injector 1.

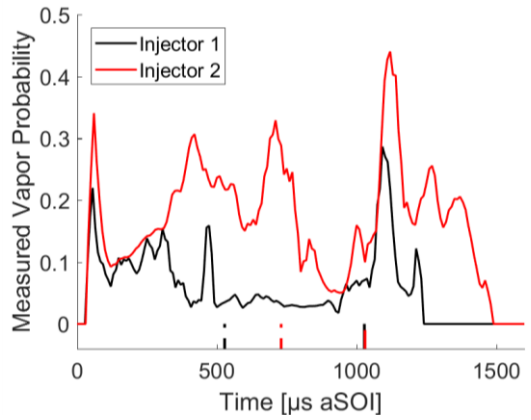

Figure 6. Comparison of time-varying vapor probability for two different injector tip geometries (both with HEO) at 300 bar injection pressure and 15 bar ambient pressure.

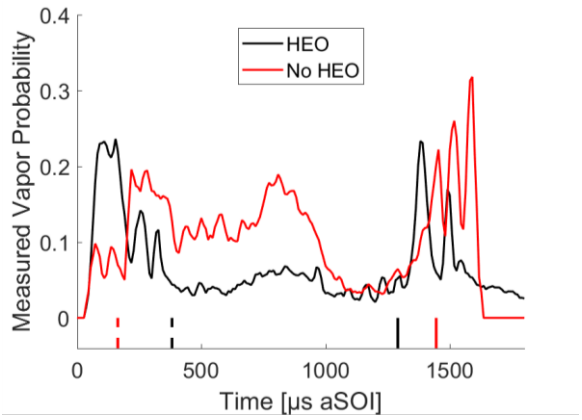

Figure 7. Comparison of time-varying vapor probability for Injector 1 with and without HEO at 400 bar Injection pressure and 15 bar ambient pressure.

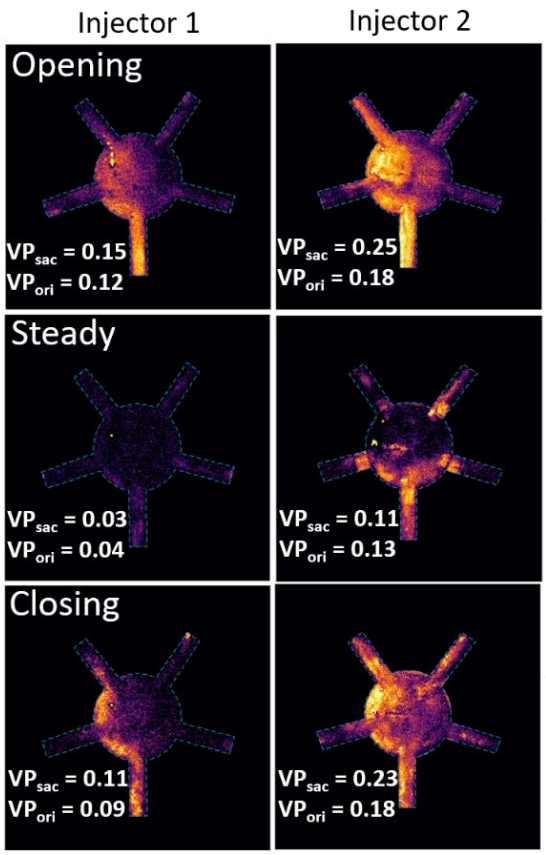

Figure 8. Measured spatial vapor probability (VP) maps compared for differing injector geometries during three periods of injection at 300 bar. Ambient pressure is 15 bar.

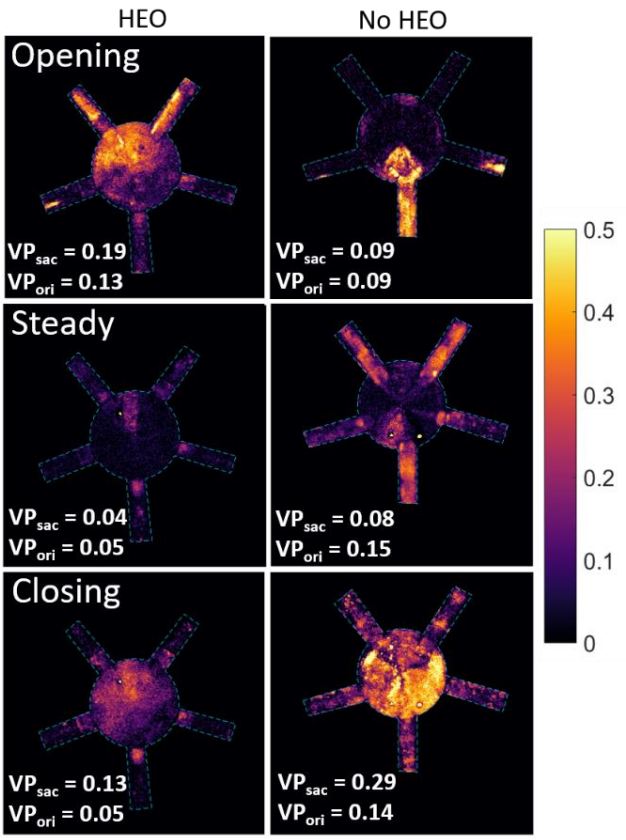

Figure 9. Measured spatial vapor probability (VP) maps compared for Injector 1 with and without HEO during three periods of injection at 400 bar. Ambient pressure is 15 bar.

Effects of orifice inlet radius rounding via hydro-erosive grind on vapor probability and distribution are shown for Injector 1 in Figures 7 and 8. Apparently, the sharp orifice inlet radius for the non-HEO case has a diminishing effect on the opening period as evidenced by very fast sac clearing (i.e. less than 200µs) and relatively low vapor probability (9%) in the holes and orifices. Nevertheless, during steady state, lack of HEO results in three times higher vapor probability in the orifices as shown in Figure 9. For this case, vapor inception is observed near the orifice inlet with the bubble cloud spanning the length of the hole for three out of five orifices.

Ambient Pressure Effects

To examine the effect of doubling the ambient pressure on vapor inception, internal flow features and statistics are compared in Figures 10 and 11 for Injector 2, which is known to exhibit high vapor probability and cavitation erosion damage. As ambient pressure is further increased above the fluid vapor pressure, and flow potential is decreased, cavitation is expected to diminish according to Eq. 1. At 300 bar injection pressure, as ambient pressure increases from 15 bar to 30 bar, the cavitation number increases from 1.05 to 1.11 as illustrated in Figure 3. Consistent with expectations, higher ambient pressure decreases vapor probability in all sac and orifice regions throughout the injection event as shown in Figures 10 and 11; the sac clearing time is also modestly reduced. Differences in vapor probability are most pronounced during closing when the ambient communicates with the sac as gases are ingested into the injector tip. Differences are least pronounced in the sac near the end of the steady portion of injection. It is noteworthy that an injector highly prone to cavitate is nevertheless sensitive to relatively small changes in cavitation number.

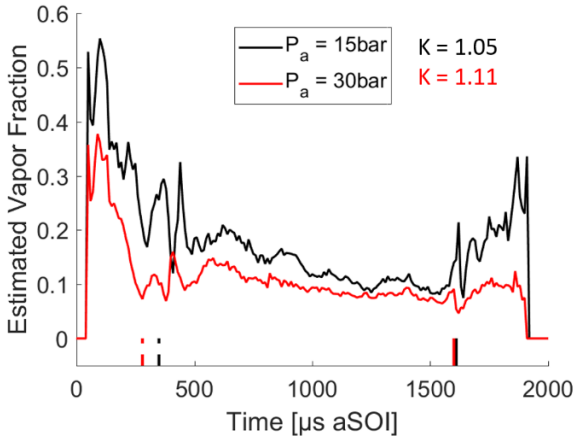

Figure 10. Comparison of time-varying vapor probability at two different ambient (back) pressures for Injector 2. Injection pressure is 300 bar.

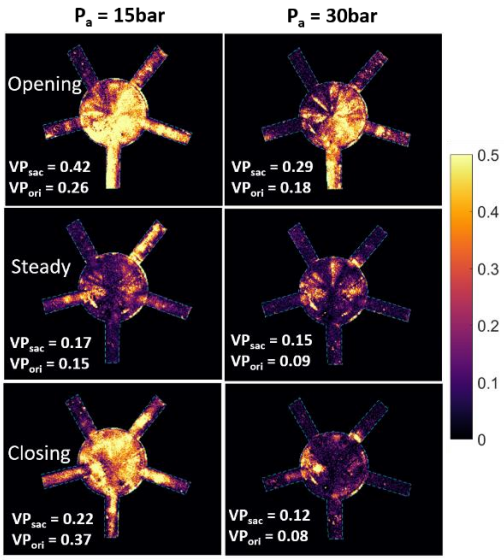

Figure 11. Vapor probability maps compared for Injector 2 operating at two different ambient pressures. Injection pressure is 300 bar.

Injection Pressure Effects

Trends with increasing injection pressure are of interest since elevated levels are known to exacerbate cavitation. Since transparent tip visualization in this work is constrained to relatively low injection pressures, i.e., well below peak operating levels, results shown in Figures 5 and 12 will be carefully considered to determine if extrapolation is reasonable.

As injection pressure is increased from 400bar to 1000bar for Injector 1, the *similarities* in the time-varying vapor probability (Figure 5) and spatial distributions (Figure 12) are striking. Vapor probabilities are not *profoundly* different despite the 2.5 factor increase in injection pressure. Sac clearing times are also similar. Modest differences may be attributed to time-differences required to lift the needle. For low injection pressures, the flow remains throttled as the needle is unlikely to achieve full lift; consequently, sac clearing times only differ by 100μs as injection pressure increases from 400 to 1000 bar. Careful examination of Figure 12 also reveals that the spatial locations of high vapor probability are generally consistent over the entire pressure range tested, particularly for the steady and closing periods. During the steady period, small regions just downstream of the orifice inlets exhibit vapor inception 5-10% of the time. These vapor clouds, which appear in Figure 4d, are generally distributed evenly downstream in the core of the orifice inlet and terminate less than a diameter downstream; this feature persists from 400 bar to 1000 bar as shown in Figure 12. Similar invariant trends are also present during the closing period, for which likeliest vapor locations *and* vapor probabilities do not change significantly with injection pressure. As the needle begins to close, the influence of injection pressure begins to diminish, and ambient pressure effects become more significant (as discussed with Figures 10 and 11); consequently, overall vapor probabilities in the sac and orifices are generally invariant with injection pressure as indicated by the inset statistical summaries.

Statistical trends in integrated vapor probability in the sac and orifices for Injector 1 at 15 bar ambient pressure are listed for varying injection pressure as insets in Figure 12. In general, results confirm that vapor is more likely to form in the sac than the orifices during opening and closing; whereas vapor is more likely to form in the orifices during the steady portion of injection. As injection pressure increases from 400 to 1000bar, the cavitation number declines from 1.051 to 1.017 as indicated on the red curve of Figure 3. This increased propensity to cavitate manifests itself as a monotonic increase in the measured vapor probability in both the sac and orifices during the opening and steady periods of injection. Significantly, these results demonstrate that cavitation number is a key indicator of the relative quantity of vapor inception for these complex multi-dimensional flows; whereas, the *location* of highest vapor quantity is apparently dominated by injector tip geometry.

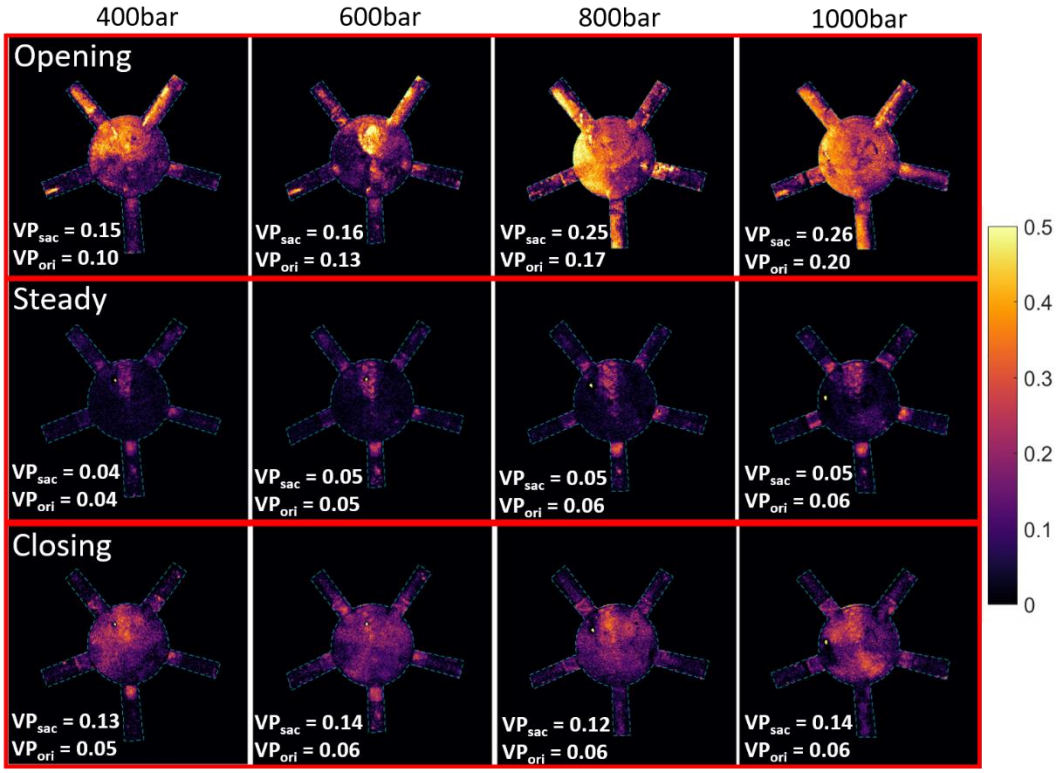

Figure 12. Vapor probability maps compared for Injector 1 operating at four different rail pressures during three periods of injection. Ambient pressure is 15 bar.

Effects on Spray

Some general effects of internal flow and cavitation on spray formation and propagation in a quiescent constant pressure vessel are briefly summarized in Figure 13. Sprays from metal (non-transparent, without counterbores) versions of Injectors 1 and 2 have been tested at a condition that mimics engine operation (P_i = 1600 bar and P_a = 60 bar) as denoted by the black 'X' in Figure 3. This condition has a higher propensity to cavitate than the transparent tip conditions investigated in Figure 6; however, comparison of the curves in Figure 13 show only subtle differences in spreading angle and vapor penetration despite differences in the needle/seat geometry. During the opening phase, the cavitating spray (Injector 2) requires about 100μs longer to establish a quasi-steady spreading angle – a trend consistent with longer times required for sac clearing. Once established, the spreading angle is as much as 0.5º degrees wider – a possible consequence of the periodic disruption of dense fluid in the jet exiting the orifice – which could have an impact on early mixing and ignition delay. Notably, a widening of the jet leaving the transparent tip orifice was observed periodically at instances when string cavitation and vapor clouds were also present in the orifice. The spread of dashed lines during the opening phase for the top plot of Figure 13 also indicate that orifice to orifice variations are measurably higher for the strongly cavitating Injector 2. Nevertheless, these apparent differences are small. Vapor penetration is nearly identical for the two injectors at these conditions, demonstrating that fuel jet propagation and mixing are likely dominated by momentum and external flow processes, rather than by upstream internal processes near the sac entrance for this case.

Simulation Results and Discussion

Simulations of spatially varying vapor probability are compared in Figure 14 to assess model predictive capability and to better understand reasons for observed differences for injectors 1 and 2, both of which are simulated at 500 bar injection pressure and 15 bar ambient pressure. This *target transparent tip operating condition* is for a cavitation number of 1.03, corresponding to a value near the worst-case operating condition (i.e. unfilled circular points in Figure 3). All cases were simulated for: 1) the actual transparent tip as measured by x-ray tomography, and 2) ideal geometries (not shown here) to enable effects of manufacturing defects to be determined.

Many features observed for transparent tip measurements are also predicted by the simulations. The opening phase of injection exhibits the highest vapor probability, reaching values between 0.1 and 0.5 in agreement with experiments. Simulations also agree that lowest probability of vapor occurs during the steady period of injection. Small concentrated regions of vapor inception just downstream of the orifice inlet on the upper (i.e. needle) side of the sac are apparent for both injectors throughout the simulated injection event. These subtle features which are

also evident from experiments (see Figures 8, 9, and 12) do not appear in simulations using an idealized geometry, suggesting that they are an artefact of fabrication imperfections and are less likely to appear in a metal injector tip. Nevertheless, Injector 2 does uniquely exhibit a pronounced region of elevated vapor levels also downstream of the orifice inlet on the sac bottom side during the opening phase of the simulations. Similar features were observed in the experiments as seen in Figures 4d and Figure 8, although, they were more prominent during the steady phase of injection. Simulations indicate that this feature, which is a likely source of cavitation erosion, is caused by flow directed along the needle tip that must abruptly turn about the relatively sharp corner on the sac bottom side prior to entering the orifice. Simulations not explicitly shown in this work indicate that *locations* of maximum vapor probability during all phases do not significantly change as pressure is increased from 50MPa to 250MPa – consistent with the experimental observations presented in Figure 12. Surprisingly, the same simulations predict a non-monotonic increase in local vapor probability with increasing injection pressure. These findings are consistent with closing period observations described in Figure 12, but they are at odds with measurements (in the same figure) for the opening and steady periods.

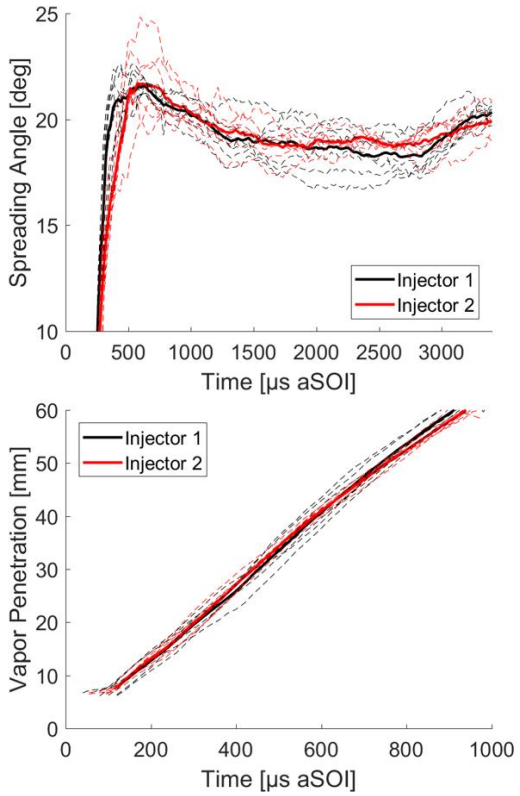

Figure 13. Comparison of spray spreading angle (top) and vapor penetration (bottom) for Injector 1 and Injector 2, both operating at P_i = 1600 bar, P_a = 60 bar, T_a = 750K. Dashed lines indicate individual spray plumes; solid lines indicate averages for all orifices.

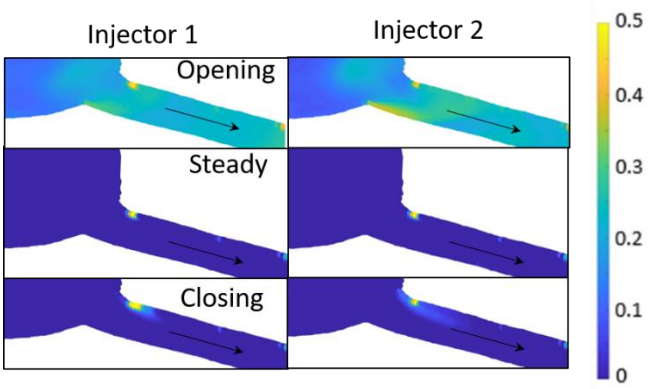

Figure 14. Comparison of simulated spatially varying vapor probability for Injectors 1 (left) and 2 (right) both operating at P_i = 500 bar and P_a = 15 bar.

Conclusions

The transparent tip visualization and vapor probability detection approaches employed in this work are sufficiently sensitive means of anticipating cavitation erosion problems in heavy duty diesel injector tips. Experiments were able to discern effects of injector tip geometry on locations and magnitude of vapor inception. Experiments, similarity analysis, and modelling results suggest that modest injection pressures and non-peak flowrates at lower ambient pressure may be sufficient for detecting and anticipating geometries that exacerbate internal flow and cavitation problems. Overall, experiments follow expected trends with changes in 1-D cavitation number, particularly during the opening and steady periods of injection; i.e., as the cavitation number tends toward unity, the local vapor probability goes up, but not precipitously. Differences in internal flow and cavitation did not *overwhelmingly* manifest themselves in spray experiments at engine relevant conditions – though subtle differences were detected as a delayed, slightly enlarged spray plume during the early stages of injection, which could impact early mixture formation and ignition delay. Simulations generally captured observed features, aiding our understanding of general effects. Remaining model deficiencies will be addressed in future work.

Acknowledgements
The authors gratefully acknowledge the laboratory contributions of Wayne Morrison and many helpful technical conversations with Tim Bazyn of Caterpillar, Inc. We also grateful acknowledge use of a high-powered LED light source for these experiments loaned by Sandia National Labs, and needle lift profiles measured by Christopher Powell and colleagues at Argonne National Laboratories Advanced Photon Source (APS).

Nomenclature

aSOI	After Start-of-Injection Time [µs]
D_{CB}	Counterbore diameter
D_{in}	Orifice inlet diameter
D_{out}	Orifice outlet diameter
K	Non-Dimensional Cavitation Number
L	Orifice length
P_a	Ambient (Back) Pressure [bar]
P_i	Injection Pressure [bar]
P_v	Diesel Vapor Pressure [bar]
T_a	Ambient Temperature [K]
VP_{sac}	Vapor Probability in Sac
VP_{ori}	Vapor Probability in Orifice

References

[1] Reitz, R., and Bracco, F., 1982, Physics of Fluids, 25, pp. 1730.
[2] Knox-Kelecy, A., and Farrell, P., 1992, Society of Automotive Engineers (SAE) Technical Paper 922308.
[3] Pierpont, D., and Reitz, R., 1995, SAE Technical Paper 922308.
[4] Koo, J., and Martin, J., 1995, Atomization and Sprays, 5 (1), pp. 107-121.
[5] Benajes, J., Pastor, J., Payri, R., and Plazas, A., 2004, J. Fluids Eng 126 (1), pp. 63-71.
[6] Desantes, J., Payri, R., Pastor, J., and Gimeno, J., 2005, Atomization and Sprays, 15 (5), pp. 489-516.
[7] Nurick, W., 1976, ASME J. Fluids Eng. 98 (4), pp. 681-687.
[8] Kim, J., Nishida, K., and Hiroyasu, H., 1997, Proc. ICLASS, pp. 175-182.
[9] Soteriou, C., Andrews, R., and Smith, M., 1995, 1995, SAE Technical Paper 950080.
[10] Soteriou, C., Andrews, R., Smith, M., Torres, N., Sankhalpara, S., 2000, SAE Technical Paper 2000-01-0943.
[11] Arcoumanis, H., Flora, M., Gavaises, M. Kampanis, N., 1999, SAE Technical paper 1999-01-0524,
[12] Arcoumanis, H., Flora, M., Gavaises, M., 2000, SAE Technical Paper 2000-01-1249.
[13] Schmidt, D., Rutland, C., and Corradini, M., 1999, SAE Technical Paper 1999-01-0518.
[14] Ning, W., and Reitz, R., SAE Technical Paper 2008-01-0936.
[15] Fitzgerald, R., and Bazyn, T., 2018, Proc. ICLASS.
[16] CONVERGE Manual, CONVERGECFD 2.4.
[17] Saha, K., Srivastava, P., Quan, S., Senecal, P., et al., 2018, SAE Technical Paper 2018-01-0314
[18] Brusiani, F., Negro, S., Bianchi, G., Moulai, M., et al., 2013, SAE Technical Paper 2013-01-1613.
[19] Swantek, A., Duke, D., Tilocco, Z., Sovis, N., et al., 2014, Proc. ILASS Americas.
[20] Manin, J., Pickett, L., and Yasutomi, K., 2018, Proc. ICLASS.
[21] Baldwin, E., Grover, R., Duke, D., Matusik, K., et al., 2016, Proc. ILASS Americas.
[22] Torelli, R., Matusik, K., Nelli, K., Kastengren, A., et al., 2018, SAE Technical Paper 2018-01-0303.